

The deep multi-FBSDE method: a robust deep learning method for coupled FBSDEs

Kristoffer Andersson^{*†}

Adam Andersson^{‡§}

Cornelis W. Oosterlee^{*}

March 18, 2025

Abstract

We introduce the deep multi-FBSDE method for robust approximation of coupled forward–backward stochastic differential equations (FBSDEs), focusing on cases where the deep BSDE method of Han, Jentzen, and E (2018) fails to converge. To overcome the convergence issues, we consider a family of FBSDEs that are equivalent to the original problem in the sense that they satisfy the same associated partial differential equation (PDE). Our algorithm proceeds in two phases: first, we approximate the initial condition for the FBSDE family, and second, we approximate the original FBSDE using the initial condition approximated in the first phase. Numerical experiments show that our method converges even when the standard deep BSDE method does not.

1 Introduction

Solving forward-backward stochastic differential equations (FBSDEs) using deep learning has emerged as a powerful technique to overcome the curse of dimensionality inherent in classical numerical methods. Han, Jentzen, and E’s seminal work [17] introduced the *deep BSDE method*, employing neural networks to approximate solutions of high-dimensional parabolic partial differential equations (PDEs) by reformulating them as FBSDEs. This breakthrough demonstrated remarkable performance on problems previously considered intractable, showcasing the ability of neural networks to efficiently handle complex nonlinearities at scales unattainable by traditional approaches. Following this success, several deep learning-based strategies have emerged, notably [6, 7, 5, 14, 28, 23, 24, 31, 19, 3], with convergence analyses provided in, *e.g.*, [18, 21, 9, 12, 16, 22, 29, 25, 2]. Concurrently, a separate branch known as backward-type methods, closer in spirit to classical dynamic programming algorithms—has developed, see *e.g.*, [20, 11, 13, 27, 26, 20, 15]. For a comprehensive overview of machine learning algorithms for PDE approximation, we refer to [8].

Despite these advancements, forward-type deep BSDE methods, including the original method by Han et al., still face significant convergence challenges when addressing certain classes of FBSDEs, such as those encountered in stochastic control problems [1]. Specifically, these forward-type approaches often fail to converge or become trapped in suboptimal solutions due to ill-conditioned optimization landscapes [20, 1, 10]. Although backward-type methods may not suffer from precisely the same convergence issues, they encounter different challenges, especially when dealing with coupled FBSDEs. The scope of this paper focuses specifically on the improvement of forward-type methods.

To address the convergence challenges, we propose a robust modification of the deep BSDE method that we name the *deep multi-FBSDE method*, applicable for a broad class of FBSDEs and their related PDEs. Our approach alleviates optimization difficulties by utilizing a family of FBSDEs that share the same initial condition as well as the same functional forms as the original FBSDE. In other words, all FBSDEs in this family are solved by the same PDE. We propose a two-phase optimization procedure. In the first phase, we approximate the joint initial conditions for all FBSDEs. In the second phase, we

^{*}Mathematical Institute, Utrecht University, Utrecht, the Netherlands

[†]Department of Economics, University of Verona. Email: kristofferherbert.andersson@univr.it

[‡]Research Group of Computational Mathematics, Chalmers University of Technology & the University of Gothenburg

[§]Saab AB, Gothenburg, Sweden

apply a reduced version of the deep BSDE method, where we optimize only over the control processes while using the initial condition obtained from the first phase. This leads to a numerical scheme which we experimentally show has consistent and accurate convergence, even for strongly coupled, nonlinear FBSDEs. Our numerical experiments demonstrate stable and accurate solutions for problems for which the classical deep BSDE methods fail.

In summary, the primary contributions of this paper are as follows.

- A robust deep FBSDE method that effectively addresses convergence issues faced by existing deep learning-based methods for strongly coupled FBSDEs.
- A general purpose training strategy applicable general FBSDE systems, without restrictive assumptions such as the existence of an equivalent stochastic control problem, as in [1].
- Comprehensive numerical demonstrations illustrating the effectiveness and robustness of our method, especially in challenging scenarios involving stochastic control and nonlinear PDEs, thus underscoring its broad applicability and efficiency.

The rest of this paper is organized as follows: Section 2 presents the FBSDE problem and its solution by the non-linear Feynann-Kac formula through the PDE. Section 3 introduces our proposed robust deep learning method, detailing its formulation and implementation. Numerical results demonstrating its advantages are presented in Section 4, and we end in Section 5 with conclusions and future directions.

2 Forward backward stochastic differential equations

Throughout this paper, we let $T \in (0, \infty)$, $d, k \in \mathbb{N}$, $x_0 \in \mathbb{R}^d$, $(W_t)_{t \in [0, T]}$ be a k -dimensional standard Brownian motion on a filtered probability space $(\Omega, \mathcal{F}, (\mathcal{F}_t)_{t \in [0, T]}, \mathbb{P})$ and the problem coefficients be denoted by $b: [0, T] \times \mathbb{R}^d \times \mathbb{R} \times \mathbb{R}^k \rightarrow \mathbb{R}^d$, $\sigma: [0, T] \times \mathbb{R}^d \rightarrow \mathbb{R}^{d \times k}$, $g: \mathbb{R}^d \rightarrow \mathbb{R}$ and $f: [0, T] \times \mathbb{R}^d \times \mathbb{R} \times \mathbb{R}^k \rightarrow \mathbb{R}$. The general form of the FBSDEs considered is given by the coupled system of equations

$$\begin{cases} X_t = x_0 + \int_0^t b(s, X_s, Y_s, Z_s) ds + \int_0^t \sigma(s, X_s) dW_s, \\ Y_t = g(X_T) + \int_t^T f(s, X_s, Y_s, Z_s) ds - \int_t^T Z_s \sigma(s, X_s) dW_s, \quad t \in [0, T]. \end{cases} \quad (1)$$

The associate PDE is then a semilinear parabolic PDE on the form

$$\begin{cases} \frac{\partial v}{\partial t}(t, x) + \mathcal{L}v(t, x) + f(t, x, v(t, x), D_x v(t, x) \sigma(t, x)) = 0, & (t, x) \in [0, T) \times \mathbb{R}^d, \\ v(t, x) = g(x), & (t, x) \in \{T\} \times \mathbb{R}^d. \end{cases} \quad (2)$$

Here \mathcal{L} is the infinitesimal generator, which when acting on a twice continuously differentiable function ρ yields

$$\begin{aligned} \mathcal{L}\rho(x) &= b(t, x, \rho(t, x), D_x \rho(t, x) \sigma(t, x))^\top D_x \rho(x) + \frac{1}{2} \text{Tr}(a(t, x) D_x^2 \rho(x)) \\ &= \sum_{i=1}^d b_i(t, x, \rho(t, x), D_x \rho(t, x) \sigma(t, x)) \partial_i \rho(x) + \frac{1}{2} \sum_{i,j=1}^d a_{ij}(t, x) \partial_{i,j} \rho(x), \end{aligned}$$

where $a = \sigma \sigma^\top$ and $\text{Tr}(\cdot)$ denotes the trace of a matrix. The connection between (1) and (2) is established through the nonlinear Feynman-Kac formula, see *e.g.*, [32], which states that

$$Y_t = v(t, X_t), \text{ and } Z_t = D_x v(t, X_t).$$

Note that in the above, we have implicitly assumed that v is differentiable with respect to the spatial variable. Although this holds true when (2) possesses a classical solution, we can often only expect a solution in the viscosity sense. In this situation, derivatives of v with respect to the space variable should be interpreted as set-valued sub-derivatives. Nevertheless, from our perspective, which is to find approximations of (1) and (2), we can overlook this obstacle and view Z as defined above.

3 The deep BSDE and deep multi-FBSDE methods

In this section, we first introduce the classical deep BSDE method and briefly discuss its convergence problems for coupled FBSDEs. Most importantly, we introduce our novel modification of the scheme. We use a linear quadratic Gaussian (LQG) problem to demonstrate both the convergence problems of the deep BSDE method and the convergence of our method. The details of the LQG problem can be found in Section 4.1.2 together complementary experimental results.

3.1 The deep BSDE method

The deep BSDE method relies on a reformulation of the FBSDE (1) into two forward SDEs, one with an a priori unknown initial value. It relies moreover on the Markov property of the FBSDE, which guarantees that $Z_t = \zeta^*(t, X_t)$, for some function $\zeta^*: [0, T] \times \mathbb{R}^d \rightarrow \mathbb{R}^k$, that we refer to as a Markov map. Optimization is done with respect to such functions and the initial values y_0 with the objective to satisfy the terminal condition. More precisely, the FBSDE (1) is reformulated into the following variational problem

$$\begin{cases} \underset{y_0, \zeta}{\text{minimize}} \mathbb{E}|Y_T^{y_0, \zeta} - g(X_T^{y_0, \zeta})|^2, & \text{where} \\ X_t^{y_0, \zeta} = x_0 + \int_0^t b(s, X_s^{y_0, \zeta}, Y_s^{y_0, \zeta}, Z_s^{y_0, \zeta}) ds + \int_0^t \sigma(s, X_s^{y_0, \zeta}) dW_s, \\ Y_t^{y_0, \zeta} = y_0 - \int_0^t f(s, X_s^{y_0, \zeta}, Y_s^{y_0, \zeta}, Z_s^{y_0, \zeta}) ds + \int_0^t Z_s^{y_0, \zeta} \sigma(s, X_s^{y_0, \zeta}) dW_s, \\ Z_t^{y_0, \zeta} = \zeta(t, X_t^{y_0, \zeta}), \quad t \in [0, T]. \end{cases} \quad (3)$$

Here y_0 and ζ are sought in appropriate spaces. It is clear that setting $y_0 = Y_0$ and $\zeta = \zeta^*$ yields a minimizer of the objective function which attains zero and hence, solves (3). Moreover, assuming well-posedness and sufficient regularity of (1), existence and uniqueness of the minimizer are guaranteed. The connection between (1) and (2) yields $y_0^* = Y_0 = v(0, x_0)$ and $\zeta^* = Z = D_x v$.

We obtain a semi-discretized version of (3) by approximating the Itô integrals using the Euler-Maruyama scheme. We assume an equidistant temporal grid with $N \in \mathbb{N}$ time steps given by $\pi = \{t_0, t_1, \dots, t_N\}$ with $t_0 = 0$, $t_N = T$ and step size $h = t_{n+1} - t_n$, and denote the *i.i.d.* Wiener increments by $\Delta W_n = W_{t_{n+1}} - W_{t_n} \sim \mathcal{N}(0, h)$. The semi-discrete version of (3) is given by:

$$\begin{cases} \underset{y_0, \zeta_0, \dots, \zeta_{N-1}}{\text{minimize}} \mathbb{E}|Y_N^{h, y_0, \zeta} - g(X_N^{h, y_0, \zeta})|^2, & \text{where} \\ X_{n+1}^{h, y_0, \zeta} = X_n^{h, y_0, \zeta} + b(t_n, X_n^{h, y_0, \zeta}, Y_n^{h, y_0, \zeta}, Z_n^{h, y_0, \zeta})h + \sigma(s, X_n^{h, y_0, \zeta})\Delta W_n, \\ Y_{n+1}^{h, y_0, \zeta} = Y_n^{h, y_0, \zeta} - f(t_n, X_n^{h, y_0, \zeta}, Y_n^{h, y_0, \zeta}, Z_n^{h, y_0, \zeta})h + Z_n^{h, y_0, \zeta} \sigma(t_n, X_n^{h, y_0, \zeta})\Delta W_n, \\ Z_n^{h, y_0, \zeta} = \zeta_n(X_n^{h, y_0, \zeta}), \quad Y_0^{h, y_0, \zeta} = y_0, \quad X_0^{h, y_0, \zeta} = x_0, \quad n \in \{0, 1, \dots, N-1\}. \end{cases} \quad (4)$$

In the deep FBSDE method, we search for $y_0 \in \mathbb{R}$, a simple trainable parameter, and for $n \in 0, \dots, N-1$, ζ_n in a parametric space defined by the architecture of a specified neural network.

In [18] an a posteriori error analysis of (4) is provided under certain, rather restrictive assumptions. The full simulation error for the FBSDE can be bounded (up to a constant) by the time step h and an a posteriori term given by the mean-squared error of the discrete terminal condition. Concretely, there exists a constant C , independent of h , such that for sufficiently small h

$$\sup_{t \in [0, T]} \mathbb{E}|X_t - \hat{X}_t^{h, y_0, \zeta}|^2 + \sup_{t \in [0, T]} \mathbb{E}|Y_t - \hat{Y}_t^{h, y_0, \zeta}|^2 + \mathbb{E} \left[\int_0^T |Z_t - \hat{Z}_t^{h, y_0, \zeta}|^2 dt \right] \leq C(h + \mathbb{E}|\hat{Y}_N^{h, y_0, \zeta} - g(X_N^{h, y_0, \zeta})|^2), \quad (5)$$

where for $n \in \{0, 1, \dots, N-1\}$, and $t \in [t_n, t_{n+1})$ we have defined

$$\hat{X}_t^{h, y_0, \zeta} = X_n^{h, y_0, \zeta}, \quad \hat{Y}_t^{h, y_0, \zeta} = Y_n^{h, y_0, \zeta}, \quad \hat{Z}_t^{h, y_0, \zeta} = Z_n^{h, y_0, \zeta}.$$

Under conditions that guarantee the same or similar a posteriori bound, such as those in [18], the function $\mathbb{E}|\hat{Y}_N^{h, y_0, \zeta} - g(X_N^{h, y_0, \zeta})|^2$ is a highly suitable loss function and guarantees an approximation

with an error bounded by the loss after training and the time step. When the assumptions are not met, the situation is less fortunate. Counterexamples of FBSDE from stochastic control are presented in [1] for which it is possible to make the right-hand side of (5) arbitrarily small, but with the left-hand side remaining large and discrete solutions converging to severely wrong processes. In this paper, we provide four more counterexamples. Thus, while the a posteriori bound in [18] is a powerful tool under its specific conditions, extrapolating it beyond these conditions is a shaky practice.

For instructive purposes and since we address the convergence problem documented in [1], with a novel method, we briefly repeat the problem with a numerical example. In order to demonstrate that the optimization landscape for the deep BSDE method is problematic for strongly coupled FBSDEs, we use the mean-squared error (MSE)

$$\text{MSE}(y_0) := \inf_{\zeta} \mathbb{E}[|Y_N^{h,y_0,\zeta} - g(X_N^{h,y_0,\zeta})|^2]. \quad (6)$$

This is the MSE with y_0 fixed and only ζ being optimized. If joint optimization of y_0 and ζ , as in the deep BSDE method, is supposed to yield a good approximation of the FBSDE, then by necessity the minimum of $y_0 \mapsto \text{MSE}(y_0)$ must be close to the true Y_0 of the FBSDE. For an LQG problem, detailed in Section 4.1.2 below, Figure 1 shows that the optimization landscape $y_0 \mapsto \text{MSE}(y_0)$ instead has a minimum y_0^* very far from the true Y_0 . Figure 2 shows the exact Y and the output of the deep FBSDE method, pathwise and in mean. We note that although the initial condition is significantly incorrect, the terminal condition is well approximated, i.e., $g(X_N^{h,y_0,\zeta}) - Y_N^{h,y_0,\zeta}$ is small both on the pathwise level and in the mean-squared sense. It should be noted that the numerical algorithm has converged, as the loss function is no longer decreasing and y_0 remains constant (not shown here but Figure 6 qualitatively shows the same behavior for a different problem). Moreover, the algorithm is stable, with repeated runs yielding similar values for the loss function and y_0 . The reader might wonder if a smaller time step h in the approximation would improve approximation of Y_0 . Figure 5 gives a negative answer to this valid thought by showing non-convergence (the case $K = 1$ in that figure).

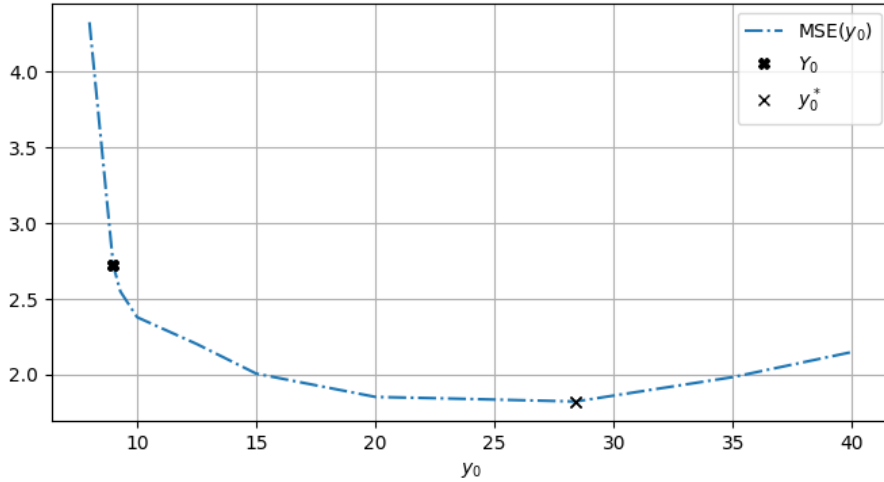


Figure 1: MSE plotted for different values of y_0 for the LQG-problem of Section 4.1.2.

The behavior depicted in Figures 1–2 is not confined to a narrow class of specific problems or special cases. For example, it is not limited to strongly coupled FBSDEs, and one can easily construct low-dimensional (e.g., $d = 2$) examples of decoupled BSDEs with smooth solutions to the associated PDE, wherein the deep BSDE method fails. In particular, quadratic BSDEs appear susceptible to this phenomenon. A more detailed, although mostly qualitative and empirical, discussion of the reasons for this lack of convergence is provided in [1].

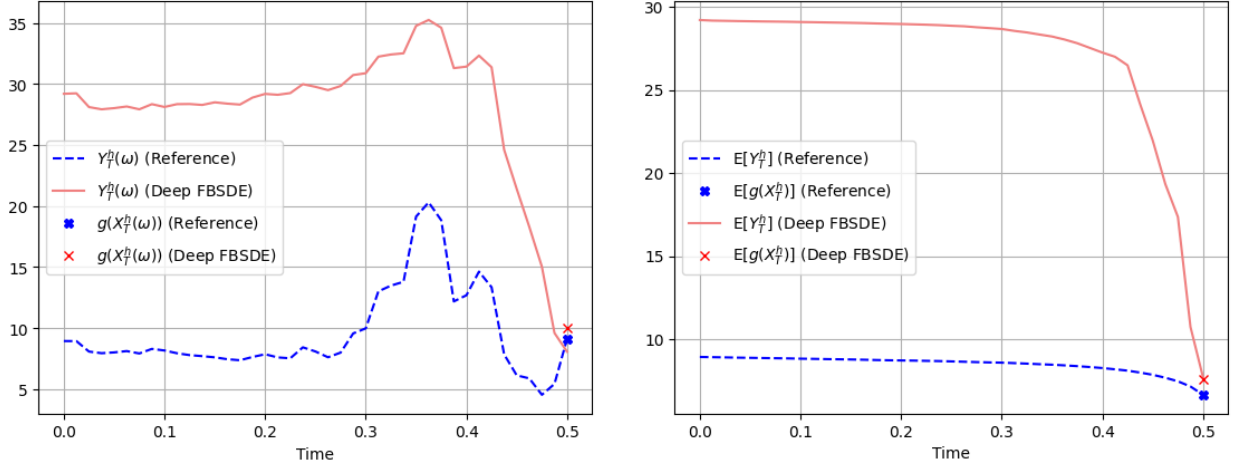


Figure 2: The almost analytical Y -process and the approximation obtained by using the deep FBSDE method. **Left:** One representative path. **Right:** A sample mean of size 2^{12} .

3.2 The deep multi-FBSDE method

Our deep multi-FBSDE method is based on a slightly modified variational formulation. To arrive at it, we notice that for sufficiently regular $\psi: [0, T] \times \mathbb{R}^d \times \mathbb{R} \times \mathbb{R}^\ell \rightarrow \mathbb{R}^d$, it holds by the Itô formula, for $Y_t^\psi = v(t, X_t^\psi)$ and $Z_t^\psi = D_x v(t, X_t^\psi)$ that

$$\begin{cases} X_t^\psi = x_0 + \int_0^t (b(s, X_s^\psi, Y_s^\psi, Z_s^\psi) - \psi(s, X_s^\psi, Y_s^\psi, Z_s^\psi)) ds + \int_0^t \sigma(s, X_s^\psi) dW_s, \\ Y_t^\psi = g(X_T^\psi) + \int_t^T (f(s, X_s^\psi, Y_s^\psi, Z_s^\psi) - \langle \psi(s, X_s^\psi, Y_s^\psi, Z_s^\psi), Z_s^\psi \rangle) ds \\ \quad - \int_t^T Z_s^\psi \sigma(s, X_s^\psi) dW_s, \quad t \in [0, T]. \end{cases} \quad (7)$$

This defines a family of FBSDEs, indexed by ψ , which are all equivalent to the PDE (2). In particular, for all ψ we have $Y_0^\psi = v(0, X_0^\psi) = v(0, x_0)$ and thus the initial value is shared for all ψ , which we utilize. Introducing the shorthand notation

$$\begin{aligned} b^\psi(t, x, y, z) &:= b(t, x, y, z) - \psi(t, x, y, z) \\ f^\psi(t, x, y, z) &:= f(t, x, y, z) - \langle z, \psi(t, x, y, z) \rangle, \end{aligned}$$

we have for any ψ the variational formulation

$$\begin{cases} \text{minimize}_{y_0, \zeta} \mathbb{E} |Y_T^{y_0, \zeta, \psi} - g(X_T^{y_0, \zeta, \psi})|^2, \quad \text{where} \\ X_t^{y_0, \zeta, \psi} = x_0 + \int_0^t b^\psi(s, X_s^{y_0, \zeta, \psi}, Y_s^{y_0, \zeta, \psi}, Z_s^{y_0, \zeta, \psi}) ds + \int_0^t \sigma(s, X_s^{y_0, \zeta, \psi}) dW_s, \\ Y_t^{y_0, \zeta, \psi} = y_0 - \int_0^t f^\psi(s, X_s^{y_0, \zeta, \psi}, Y_s^{y_0, \zeta, \psi}, Z_s^{y_0, \zeta, \psi}) ds + \int_0^t Z_s^{y_0, \zeta, \psi} \sigma(s, X_s^{y_0, \zeta, \psi}) dW_s, \\ Z_t^{y_0, \zeta, \psi} = \zeta(t, X_t^{y_0, \zeta, \psi}), \quad t \in [0, T]. \end{cases} \quad (8)$$

Since the optimal y_0^* and ζ^* are optimal for all ψ , we trivially have, for $K \in \mathbb{N}$, $\psi_1, \dots, \psi_K: [0, T] \times \mathbb{R}^d \times \mathbb{R} \times \mathbb{R}^\ell \rightarrow \mathbb{R}^d$, the equivalent variational formulation,

$$\begin{cases} \text{minimize}_{y_0, \zeta} \sum_{k=1}^K \mathbb{E} |Y_T^{y_0, \zeta, \psi_k} - g(X_T^{y_0, \zeta, \psi_k})|^2, & \text{where for } \psi \in \{\psi_1, \dots, \psi_K\} \\ X_t^{y_0, \zeta, \psi} = x_0 + \int_0^t b^\psi(s, X_s^{y_0, \zeta, \psi}, Y_s^{y_0, \zeta, \psi}, Z_s^{y_0, \zeta, \psi}) ds + \int_0^t \sigma(s, X_s^{y_0, \zeta, \psi}) dW_s, \\ Y_t^{y_0, \zeta, \psi} = y_0 - \int_0^t f^\psi(s, X_s^{y_0, \zeta, \psi}, Y_s^{y_0, \zeta, \psi}, Z_s^{y_0, \zeta, \psi}) ds + \int_0^t Z_s^{y_0, \zeta, \psi} \sigma(s, X_s^{y_0, \zeta, \psi}) dW_s, \\ Z_t^{y_0, \zeta, \psi} = \zeta(t, X_t^{y_0, \zeta, \psi}), \quad t \in [0, T]. \end{cases} \quad (9)$$

The deep multi-FBSDE is divided into two phases. Phase I is based on approximating (9) for suitable K and ψ_1, \dots, ψ_K , with time discretization, neural network approximation of ζ and stochastic gradient descent. In the second phase, a better approximation of ζ is obtained by solving the classical deep BSDE method with the exception that only ζ is optimized and y_0 is taken from Phase I. For easy and low-dimensional problems, Phase I gives an accurate approximation of ζ and Phase II is not needed. For more challenging and high-dimensional problems, we have observed that Phase II improves the approximation accuracy. We believe that this has to do with the fact that in Phase I the Markov map ζ is optimized for good fit along typical trajectories of K different SDEs, i.e., in a larger domain than in Phase II, where it is only trained along typical trajectories of the original forward SDE, i.e., for a more limited task.

We next state the scheme and similar to the deep BSDE method let ζ represent $\zeta_0, \dots, \zeta_{N-1}$.

Phase I - Approximation of Y_0 :

$$\begin{cases} \text{minimize}_{y_0, \zeta_0, \dots, \zeta_{N-1}} \sum_{k=1}^K \mathbb{E} |Y_N^{h, y_0, \zeta, \psi_k} - g(X_N^{h, y_0, \zeta, \psi_k})|^2, & \text{where for } \psi \in \{\psi_1, \dots, \psi_K\} \\ X_{n+1}^{h, y_0, \zeta, \psi} = X_n^{h, y_0, \zeta, \psi} + b^\psi(t_n, X_n^{h, y_0, \zeta, \psi}, Y_n^{h, y_0, \zeta, \psi}, Z_n^{h, y_0, \zeta, \psi}) h + \sigma(s, X_n^{h, y_0, \zeta, \psi}) \Delta W_n, \\ Y_{n+1}^{h, y_0, \zeta, \psi} = Y_n^{h, y_0, \zeta, \psi} - f^\psi(t_n, X_n^{h, y_0, \zeta, \psi}, Y_n^{h, y_0, \zeta, \psi}, Z_n^{h, y_0, \zeta, \psi}) h + Z_n^{h, y_0, \zeta, \psi} \sigma(t_n, X_n^{h, y_0, \zeta, \psi}) \Delta W_n, \\ Z_n^{h, y_0, \zeta, \psi} = \zeta_n(X_n^{h, y_0, \zeta, \psi}), \quad X_0^{h, y_0, \zeta, \psi} = x_0, \quad Y_0^{h, y_0, \zeta, \psi} = y_0, \\ \text{for } n \in \{0, 1, \dots, N-1\}, \end{cases} \quad (10)$$

Phase II - Approximation of the full FBSDE with known initial value:

$$\begin{cases} \text{minimize}_{\zeta_0, \dots, \zeta_{N-1}} \mathbb{E} |Y_N^{h, \zeta} - g(X_N^{h, \zeta})|^2, & \text{where} \\ X_{n+1}^{h, \zeta} = X_n^{h, \zeta} + b(t_n, X_n^h, Y_n^{h, \zeta}, Z_n^h) h + \sigma(s, X_n^{h, \zeta}) \Delta W_n, \\ Y_{n+1}^{h, \zeta} = Y_n^{h, \zeta} - f(t_n, X_n^{h, \zeta}, Y_n^{h, \zeta}, Z_n^{h, \zeta}) h + Z_n^{h, \zeta} \sigma(t_n, X_n^{h, \zeta}) \Delta W_n, \\ Z_n^{h, \zeta} = \zeta_n(X_n^{h, \zeta}), \quad Y_0^{h, \zeta}(m) = y_0^*, \quad \text{for } n \in \{0, 1, \dots, N-1\}, \end{cases} \quad (11)$$

We demonstrate the new numerical scheme on the LQG-problem, detailed in Section 4.1.2, for which the deep BSDE method was shown to fail in Section 3.1. In Phase I, we take $K = 1, 2, 3, 4$, with the choices $\psi_1 = 0$, $(\psi_1, \psi_2) = (0, b_1)$, $(\psi_1, \psi_2, \psi_3) = (0, b_1, -b_1)$ and $(\psi_1, \psi_2, \psi_3, \psi_4) = (0, b_1, -b_1, -0.5b_1)$, where the drift has the form $b(x, y, z) = b_1(x) + b_2(z)$, and plot the MSE curves in Figure 3. For $K = 2, 3, 4$ the optimization landscape is much more satisfactory than for $K = 1$, which is the deep BSDE method. In fact the minima are close to the real $Y_0 = 8.94$. To further indicate that the method is robust to the choice of $K \geq 3$ (and possibly $K = 2$) and (ψ_1, \dots, ψ_K) we take $K = 3$ and rather arbitrary choices $\psi_1 = b_1 \circ \xi$, $\psi_2 = -b_1 \circ \xi$, $\psi_3 = 0$, for $\xi \in \{x, -\sin(x), x \cos(x), 1 - \exp((x \wedge 1) \vee (-1))\}$, where ξ acts coordinate-wise on vectors. We obtain the four loss surfaces in Figure 4, which, based on visual inspection, have the same minima. This robustness is a very important property because when the method is applied to a problem without a reference solution, one must be able to trust that

the choice of ψ_1, ψ_2, ψ_3 does not need to be tuned based on comparison with a reference solution. Our results indicate a robustness in the choice of $K \geq 2$ and (ψ_1, \dots, ψ_K) , but it needs to be investigated further, particularly theoretically. The deviation between Y_0 and the optimized y_0^* is the discretization error due to the time stepping. This is seen empirically in the convergence plot in Figure 5 for $\xi(x) = x$, showing the experimental convergence order one, i.e., $|Y_0 - y_0^*(h)| = \mathcal{O}(h)$. The convergence of (X, Y, Z) as processes after Phase II is shown in Section 4.1.2.

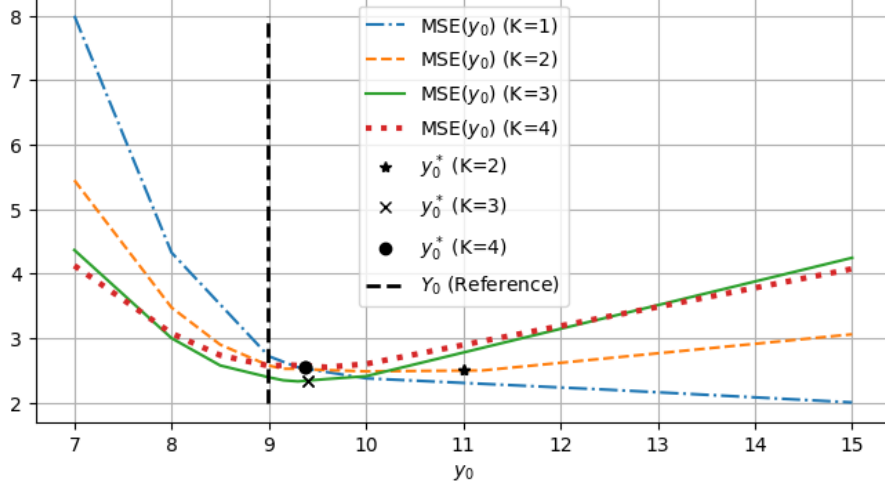


Figure 3: Four MSE curves plotted for $K = 1, 2, 3, 4$, with $\psi_1 = 0$, $(\psi_1, \psi_2) = (0, b_1)$, $(\psi_1, \psi_2, \psi_3) = (0, b_1, -b_1)$ and $(\psi_1, \psi_2, \psi_3, \psi_4) = (0, b_1, -b_1, -0.5b_1)$, where $b(x, y, z) = b_1(x) + b_2(z)$. y_0^* for $K = 1$ and $K = 2$ are the initial conditions approximated with Phase I or our method. Note that for $K = 1$, $y_0^* = 28.44$ as can be visualized in Figure 1. For visualization purposes, we have scaled the curves. For $K = 1, 2, 3, 4$, the training times are approximately 400s, 500s, 600s, and 700s, respectively.

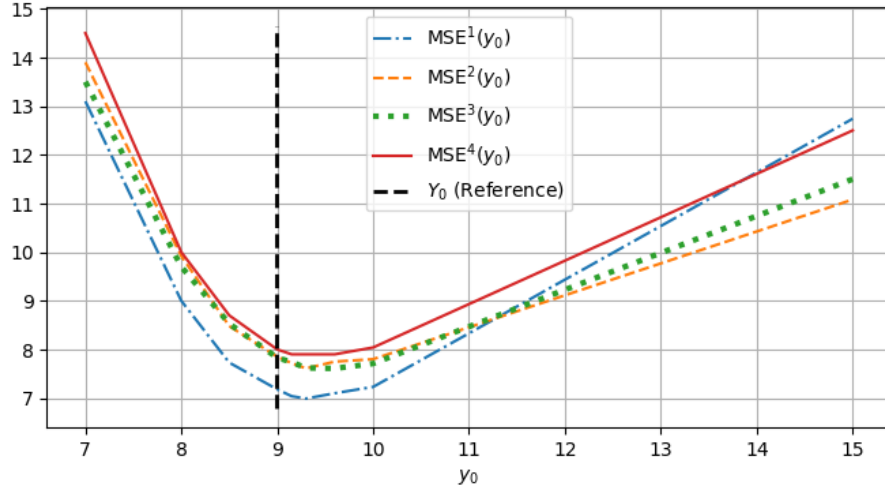


Figure 4: Four MSE curves plotted for $\psi_1 = b \circ \xi$, $\psi_2 = -b \circ \xi$, $\psi_3 = 0$, for $\xi \in \{x, -\sin(x), x \cos(x), 1 - \exp((x \wedge 1) \vee (-1))\}$, where ξ acts coordinate wise on vectors. The order coincides with that of the set.

4 Numerical experiments

We present four numerical experiments, two with an associated stochastic optimal control problem, and two without such a connection, all with analytic or semi-analytic reference solutions so that we can analyze the error. The first problem is a controlled Brownian motion in two dimensions, the

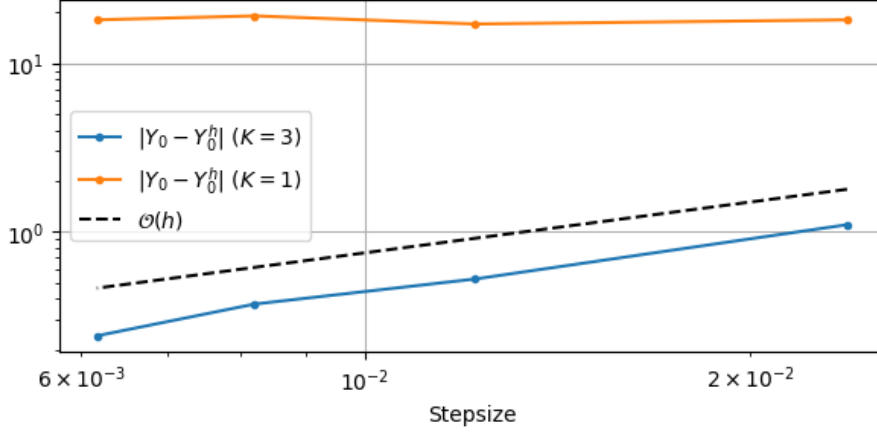


Figure 5: Empirical convergence plot for approximations of Y_0 using the deep multi-FBSDE method phase I. Here the case $K = 1$ coincides with the original deep BSDE method.

second problem is a six-dimensional LQG-problem, and the last two examples are FBSDEs related to two-dimensional advection diffusion reaction PDEs, one without a reaction term and one with a linear one. We demonstrate the performance of both the deep BSDE and the deep multi-FBSDE methods.

In the literature, it is most common to demonstrate deep BSDE-type methods on very high-dimensional problems. However, these problems are most often very symmetric, with solutions being permutation-invariant in its space variables. It is highly questionable how important these examples are for applications and also if they fairly represent more general problems of the same dimensions. We have instead chosen difficult low-dimensional problems for which the classical deep BSDE methods fail, rather than high-dimensional problems.

In the implementation of the deep BSDE and both Phase I–II of the deep multi-FBSDE methods, we optimize $\zeta_0, \dots, \zeta_{N-1}$ in a function class defined by ReLU feed-forward neural networks with 3 hidden layers with 20 nodes in each layer. The initial value y_0 in the deep BSDE method and in Phase I of the deep multi-FBSDE method is represented by one single trainable parameter. Training data consist of 2^{20} independent realizations of the d -dimensional Wiener increment vectors $\Delta W_0, \dots, \Delta W_{N-1}$, each element being *i.i.d.* and normally distributed with mean zero and variance h . The training data are reused in 10 epochs. Training is initiated by randomly sampling parameters and proceeds with the classical Adam optimizer with batches of size 2^{12} .

4.1 FBSDEs stemming from stochastic optimal control problems

In this section, we look into two main types of stochastic control problems, controlled Brownian motions and Linear Quadratic Gaussian (LQG) control problems. Before discussing these specific topics, we define the general form of the stochastic control problem:

$$\begin{cases} \underset{u}{\text{minimize}} & J(u; t, x), \quad \text{where} \\ & dX_t = b_u(t, X_t, u_t)dt + \sigma(t, X_t)dW_t, \\ & J(u; t, x) = \mathbb{E} \left[\int_t^T f_u(s, X_s, u_s)ds + g(X_T) \mid X_t = x \right], \quad t \in [0, T], \quad x \in \mathbb{R}^d. \end{cases} \quad (12)$$

Assuming existence, the value function associated with the control problem is formally defined as

$$v(t, x) = \inf_u J(u; t, x).$$

Moreover, the value function satisfies the following Hamilton–Jacobi–Bellman (HJB) equation

$$\begin{cases} \frac{\partial v}{\partial t} + \frac{1}{2} \text{Tr} \{ \sigma^\top \sigma \text{Hess}_x v \} + \inf_u [b_u^\top D_x v + f_u] = 0, & (t, x) \in [0, T) \times \mathbb{R}^d, \\ v(t, x) = g(x), & (t, x) \in T \times \mathbb{R}^d. \end{cases} \quad (13)$$

The resulting HJB-equation is a semilinear parabolic PDE of the type discussed in Section 2; therefore, it admits an equivalent formulation as an FBSDE.

4.1.1 Controlled Brownian motions with general terminal cost

In this section, we set $k = d = \ell \in \mathbb{N}$, $x_0 \in \mathbb{R}^d$, and $\sigma, r \in \mathbb{R}^+$. For $t \in [0, T]$, $x \in \mathbb{R}^d$, and $u \in \mathbb{R}^\ell$, the drift, diffusion and cost functions are defined, as follows,

$$b_u(t, x, u) = u, \quad \sigma(t, x) = \sigma I_d, \quad f(t, x, u) = \frac{r}{2}|u|^2, \quad (14)$$

together with a flexibly chosen terminal cost function $g: \mathbb{R}^d \rightarrow \mathbb{R}$. Straightforward calculations yield the optimal control for this problem $u^* = -\frac{1}{r}D_x v = -\frac{1}{r}Z$, from which we obtain the FBSDE

$$\begin{cases} X_t = x_0 - \int_0^t \frac{1}{r} Z_s ds + \sigma W_t, \\ Y_t = g(X_T) + \int_t^T \frac{1}{2r} |Z_s|^2 ds - \int_t^T \sigma Z_s dW_s, \quad t \in [0, T]. \end{cases} \quad (15)$$

Using the Cole–Hopf transformation, the solution to the above FBSDE is for $t \in [0, T]$, recovered as

$$Y_t = -\frac{1}{r\sigma^2} \log \left\{ \mathbb{E} \left[e^{-r\sigma^2 g(X_t + \xi \sqrt{T-t})} | X_t \right] \right\}, \quad (16)$$

where ξ is a standard d -dimensional normally distributed random vector.

The FBSDE (15) can then be estimated using Monte Carlo sampling. It is important to note that, in approximating $(Y_t(\omega))_{t \in [0, T]}$, nested expectations along the trajectory of $(X_t(\omega))_{t \in [0, T]}$ are required. Moreover, since X is coupled with Z in the drift component, straightforward application of this strategy for approximating Y at times other than $t = 0$ (which is independent of X 's trajectory) is challenging. However, if our approximation of (X, Y, Z) is accurate, it should follow that our approximation of Y aligns with the Monte Carlo approximation of Y using (16), along the simulated trajectories of X .

Problem Specific Settings:

For the deep multi-FBSDE method, we opt for $K = 2$, setting $\psi_1(t, x, y, z) = 0$ and $\psi_2(t, x, y, z) = \frac{r^2}{2r_2} z$. This configuration implies that $(X^{\psi_1}, Y^{\psi_1}, Z^{\psi_1})$ is the solution to (15), whereas $(X^{\psi_2}, Y^{\psi_2}, Z^{\psi_2})$ satisfies the following decoupled equation:

$$\begin{cases} X_t^{\psi_2} = x_0 + \sigma W_t, \\ Y_t^{\psi_2} = g(X_T^{\psi_2}) - \int_t^T \frac{1}{2r} |Z_s^{\psi_2}|^2 ds - \int_t^T \sigma Z_s^{\psi_2} dW_s, \quad t \in [0, T]. \end{cases} \quad (17)$$

For this relatively straightforward problem, we have observed that only the first phase of the deep multi-FBSDE method is necessary, so Phase II is skipped.

We set $T = 0.5$, $d = \ell = k = 2$, $r = 1$, and $\sigma = 0.25$. The initial state is set at $x_0 = (-0.1, 0.1)^\top$. We employ a terminal cost function $g(x) = -|x_1 - x_2|$. This configuration aims to control the two components of the Brownian motion such that they diverge as much as possible by the time $t = T$, while minimizing the use of control force. The discretization of the problem is set with $N = 40$.

Results and discussion:

Figure 6 illustrates the loss and the approximation of Y_0 during training for both the deep FBSDE method and the deep multi-FBSDE method. Notably, while the loss approaches zero for both methods, only the deep multi-FBSDE method accurately converges to the true Y_0 .

While the deep FBSDE method fails to converge to the true solution, the reason behind this discrepancy remains unclear. To further explore this discrepancy, we illustrate in Figure 7 the sample mean of the forward SDE along with a representative path of the backward SDE, comparing these

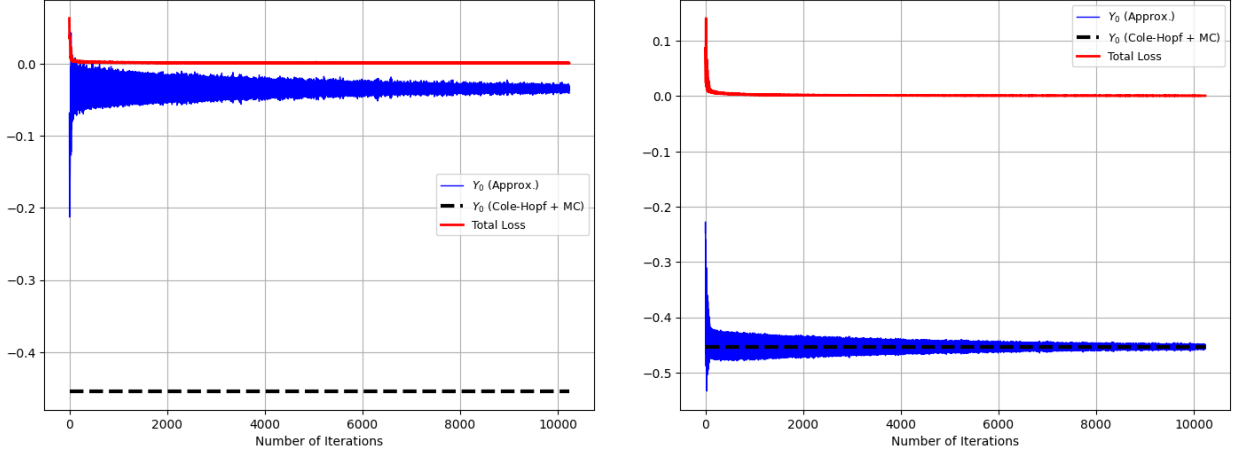


Figure 6: Loss and Y_0 during training for the deep FBSDE method (left) and the deep multi-FBSDE method (right). "Number of iterations" refers to gradient updates. The losses of the first two iterations were removed due to large values and for better visual representation.

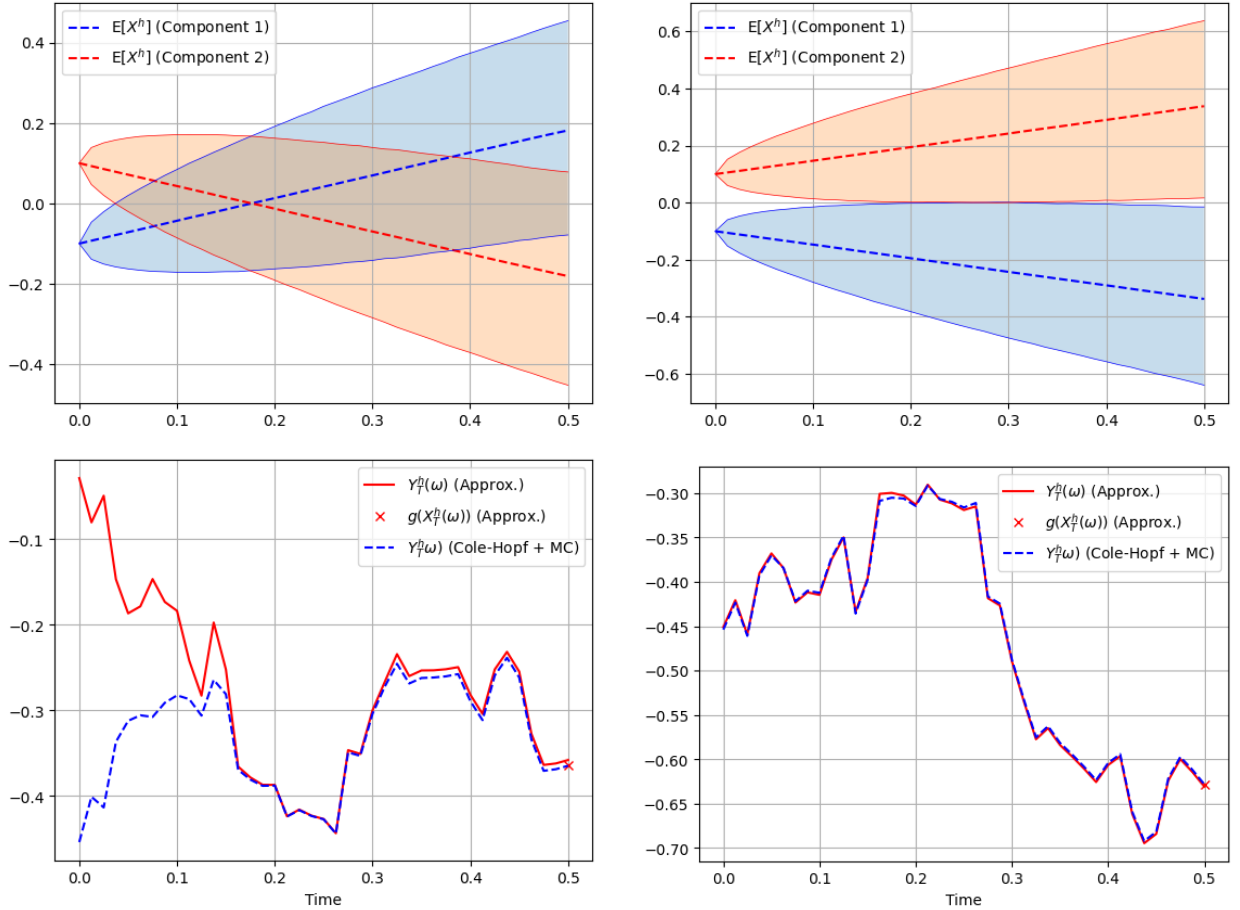


Figure 7: The upper plots display the empirical mean of X as well as the 95th and 5th percentiles for the deep FBSDE method (left) and the deep multi-FBSDE method (right). The lower plots show a representative trajectory of the approximate Y for the deep FBSDE method (left) and the deep multi-FBSDE method (right), compared with their semi-analytic counterparts.

with a reference solution computed using the Cole–Hopf transformation and Monte Carlo sampling. Intuitively, the optimal strategy should be to direct X^1 downwards and X^2 upwards. This behavior is observed in the deep multi-FBSDE method, whereas the deep FBSDE method results in the opposite: X^1 is driven upwards while X^2 is driven downwards. Interestingly, around $t = 0.18$, the first component of X surpasses the second component, and from this point forward, the control actions appear nearly optimal given the state configuration. This assertion is partially supported by the trajectory of the approximate Y , which closely follows its analytic counterpart. It is important to understand that the accuracy of the analytic Y is conditioned on the trajectory of X and is subject to Monte Carlo error. It is even crucial to note that the behavior described above does not stem from a local minimum encountered during the training process. Employing a similar methodology to that used in previous sections, where the mean-squared error is calculated for various initial values of the discretized BSDE, we confirm that the observed solution represents a global minimum. Therefore, this outcome is consistent with what should be expected a priori, given the problem setup and model parameters.

4.1.2 Linear Quadratic Gaussian control problems

Among all stochastic control problems, the linear quadratic Gaussian (LQG) control problem is notably the most structured and extensively studied, see, for example, [4]. For our purposes, it presents a closed-form analytic solution, allowing us to benchmark our numerical approximations against it.

Consider the following settings: let $k = d \in \mathbb{N}$, $\ell \in \mathbb{N}$, $x_0 \in \mathbb{R}^d$, $A, \sigma \in \mathbb{R}^{d \times d}$, $R_x, G \in \mathbb{S}_+^d$, $R_u \in \mathbb{S}_+^\ell$, and $B \in \mathbb{R}^{d \times \ell}$ with full rank, alongside $C \in \mathbb{R}^d$. For $t \in [0, T]$, $x \in \mathbb{R}^d$, and $u \in \mathbb{R}^\ell$ let

$$b_u(t, x, u) = A(C - x) + Bu, \quad f_u(t, x, u) = \langle R_x x, x \rangle + \langle R_u u, u \rangle \quad g(x) = \langle Gx, x \rangle.$$

The above, together with (12), defines the state equation and cost functional for a LQG control problem. The optimal feedback control, minimizing the Hamiltonian, $\inf_{u \in U} \langle DxV, Bu \rangle + \langle R_u u, u \rangle$, is given by

$$u_t^* = -\frac{1}{2} R_u^{-1} B^T D_x v(t, X_t). \quad (18)$$

Recalling that v is the solution to the associated HJB-equation, its solution can be expressed as

$$v(t, x) = x^\top P(t)x + x^\top Q(t) + R(t), \quad (19)$$

where (P, Q, R) are the solutions to the system of ordinary differential equations,

$$\begin{cases} \dot{P}(t) - A^T P(t) - P(t)A - P(t)BR_u^{-1}B^T P(t) + R_x = \mathbf{0}_{d \times d}, \\ \dot{Q}(t) + 2P(t)AC - A^T Q(t) - P(t)BR_u^{-1}B^T Q(t) = \mathbf{0}_d, \\ \dot{R}(t) + \text{Tr}\{\sigma\sigma^\top P(t)\} + Q(t)^\top AC - \frac{1}{4}Q(t)^\top BR_u^{-1}B^\top Q(t) = 0, \quad t \in [0, T], \\ P(T) = G; \quad Q(T) = \mathbf{0}_d; \quad R(T) = 0. \end{cases}$$

We refer to the entire system colloquially as the Riccati equation, although the first equation is strictly a matrix Riccati equation. The gradient of v , $D_x v(t, x) = 2P(t)x + Q(t)$, leads to the associated FBSDE:

$$\begin{cases} X_t = x_0 + \int_0^t [A(C - X_s) - \frac{1}{2}BR_u^{-1}B^\top Z_s]ds + \int_0^t \sigma dW_s, \\ Y_t = \langle GX_T, X_T \rangle + \int_t^T (\langle R_x X_s, X_s \rangle + \frac{1}{4}\langle R_u^{-1}B^\top Z_s, B^\top Z_s \rangle)ds - \int_t^T \langle Z_s, \sigma dW_s \rangle, \quad t \in [0, T]. \end{cases} \quad (20)$$

The solution to (20) is provided by

$$Y_t = X_t^\top P(t)X_t + X_t^\top Q(t) + R(t); \quad Z_t = 2P(t)X_t + Q(t). \quad (21)$$

In our experiments, we use the Euler approximation of the Riccati equation with 160×2^7 time steps, and for X , we use 160 time steps. The processes (Y, Z) are approximated iteratively, as per (21).

Problem Specific Settings:

For the deep multi-FBSDE method, we set $K = 3$ and define $\psi_1(t, x, y, z) = A(C - x)$, $\psi_2(t, x, y, z) = -A(C - x)$, and $\psi_3(t, x, y, z) = 0$. With this configuration, we incorporate both the doubling effect (through ψ_2) and the removal of the mean-reverting term (through ψ_1). Furthermore, since ψ_3 is identically zero, the original control problem is also explicitly included in the training, which appears to have a regularizing effect on the numerical results.

The matrices used for the state equation are given by

$$A = \text{diag}([1, 2, 3, 1, 2, 3]), \quad B = \begin{pmatrix} 1 & -1 \\ 1 & 1 \\ 0.5 & 1 \\ 1 & -1 \\ 0 & -1 \\ 0 & 1 \end{pmatrix}, \quad C = \text{diag}([-0.2, -0.1, 0, 0, 0.1, 0.2]),$$

$$\sigma = \text{diag}([0.2, 1, 0.2, 1, 0.2, 1]), \quad x_0 = (0.1, 0.1, 0.1, 0.1, 0.1, 0.1)^\top, \quad T = 0.5.$$

The penalty matrices of the control problem are given by

$$R_x = \text{diag}([25, 1, 25, 1, 25, 1]), \quad R_u = \text{diag}([1, 1]), \quad G = \text{diag}([1, 25, 1, 25, 1, 25]).$$

Results and discussion:

Figure 8 clearly demonstrates that our method yields accurate approximations for (X, Y, Z) , both pathwise and in distribution. We refrain from comparing these results with those obtained via the deep BSDE method, as the latter produce completely incorrect approximations for this problem. The approximate initial condition obtained by the deep BSDE method is around 28.44, whereas the true value is approximately 9 (see Figure 1). In [30], the authors use the deep BSDE method to approximate the solution of a BSDE derived from the stochastic maximum principle for the specific problem discussed above. However, this problem is significantly less complex because, at each time t , the control process in the associated BSDE is constant in the state space. Consequently, it remains unclear to what extent this approach would generalize to more complex problems where the control process is non-constant.

Part of the numerical experiments of this problem is the convergence to Y_0 , shown in Figure 5, as the time step h tends to zero, or in the experiment for $N \in \{20, 40, 60, 80\}$ time steps. To complete the empirical convergence study, Figure 9 shows the convergence of X and Y with orders 1 and 0.5, respectively, and a decreasing error in Z without a clear rate. We note that convergence orders 1 and 0.5 are the expected rates for forward SDEs with additive and multiplicative noise, respectively. The norms for the convergence are

$$\|A\|_{\mathcal{S}_{h,M}^2(\mathbb{R}^q)} = \max_{n \in \{0,1,\dots,N\}} \left(\frac{1}{M} \sum_{m=1}^M \|A_n(m)\|^2 \right)^{\frac{1}{2}}, \quad \|A\|_{\mathcal{H}_{h,M}^2(\mathbb{R}^q)} = \frac{1}{N} \sum_{N=0}^{N-1} \left(\frac{1}{M} \sum_{m=1}^M \|A_n(m)\|^2 \right)^{\frac{1}{2}}.$$

Here, $A(m) = \{A_1(m), A_2(m), \dots, A_N(m)\}$, $m = 1, 2, \dots, M$, are *i.i.d.* realizations of some adapted stochastic processes A on the grid.

4.2 FBSDEs from advection diffusion reaction PDEs

In this section, we consider semilinear parabolic PDEs with quadratic gradient nonlinearity.

Let $a, b \in \mathbb{R}^+$, and $x_0 \in \mathbb{R}^d$. For a general function $g: \mathbb{R}^d \rightarrow \mathbb{R}$ we define

$$\begin{cases} \frac{\partial v}{\partial t}(t, x) + a\Delta v + 2b|D_x v|^2 - cv = 0, & (t, x) \in [0, T) \times \mathbb{R}^d, \\ v(t, x) = g(x), & (t, x) \in T \times \mathbb{R}^d. \end{cases} \quad (22)$$

The above PDE is structurally similar to a Hamilton–Jacobi–Bellman (HJB) equation. However, since $b > 0$, it cannot be written in the form (13), does not have an associated stochastic control problem,

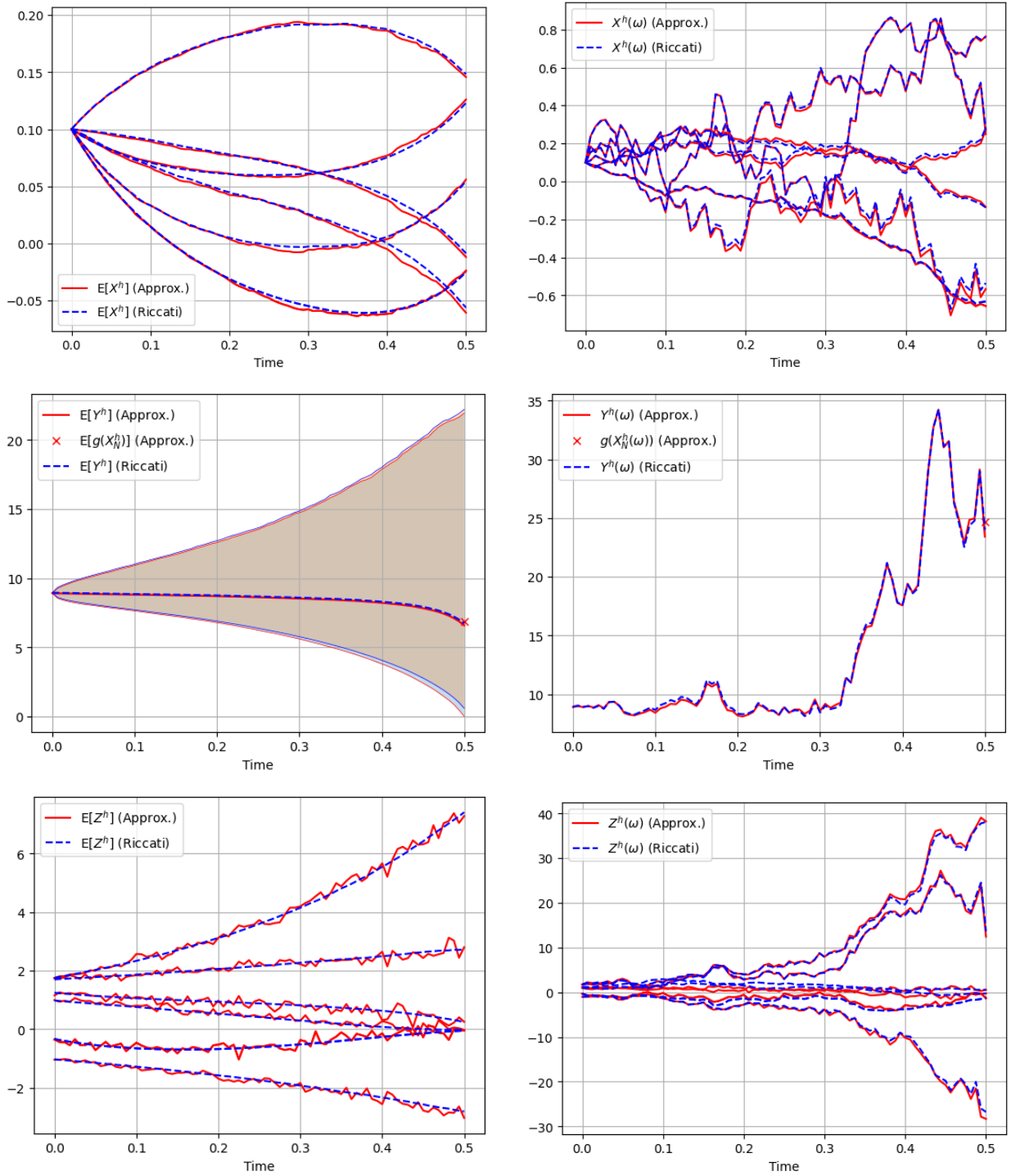


Figure 8: Average of solutions and a single solution path compared to their semi-analytic counterparts for the LQG control problem from Section 4.1.2. The shaded area represents an empirical credible interval for Y , defined as the area between the 5:th and the 95:th percentiles at each time point. We do not include credible intervals for X and Z in this figure to facilitate visualization. For X and Z , we see one realization of each of the six components.

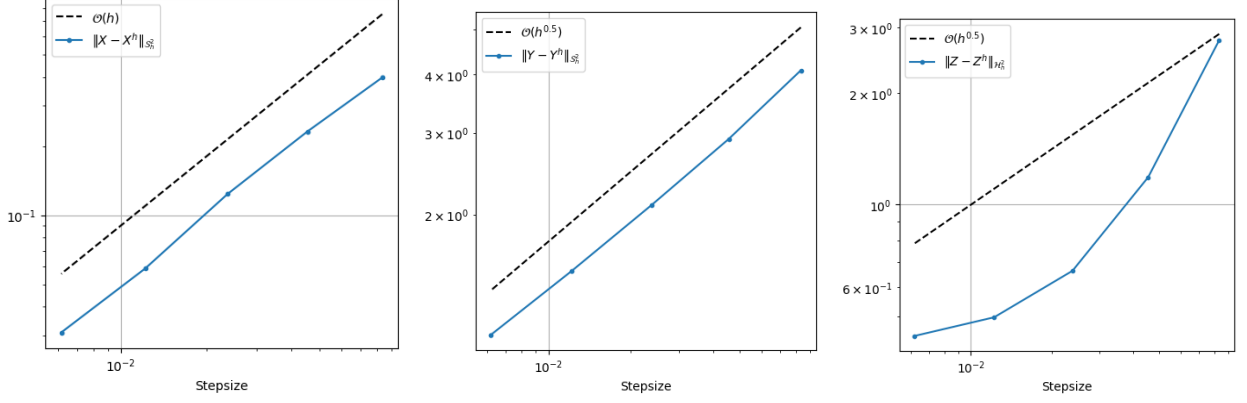


Figure 9: Empirical convergence plots for approximations of (X, Y, Z) using the deep multi-FBSDE method phase II.

and hence does not represent an HJB equation. We consider the equivalent FBSDE

$$\begin{cases} X_t = x_0 + \int_0^t b Z_s ds + \sqrt{2a} W_t, \\ Y_t = g(X_T) + \int_t^T (b |Z_s|^2 - c Y_s) ds - \int_t^T \sqrt{2a} Z_s dW_s, \quad t \in [0, T]. \end{cases} \quad (23)$$

We again employ the Cole–Hopf transformation to derive a reference solution. Specifically, defining $u(t, x) = \log \left\{ \frac{a}{2b} v(t, x) \right\}$ leads directly to the simplified PDE

$$\begin{cases} \frac{\partial u}{\partial t}(t, x) + a \Delta u - cu \log u = 0, & (t, x) \in [0, T) \times \mathbb{R}^d, \\ u(t, x) = \exp \left\{ \frac{2b}{a} g(x) \right\}, & (t, x) \in T \times \mathbb{R}^d. \end{cases} \quad (24)$$

Back transformation yields $u(t, x) = \exp \left\{ \frac{2b}{a} v(t, x) \right\}$. In the special case, $c = 0$ we have for $t \in [0, T]$

$$Y_t = -\frac{2b}{a} \log \left\{ \mathbb{E} \left[e^{-\frac{a}{2b} g(X_t + \xi \sqrt{T-t})} | X_t \right] \right\}, \quad (25)$$

where ξ is a standard d -dimensional normally distributed random vector.

Problem Specific Settings:

For the deep multi-FBSDE method, we opt for $K = 2$, setting $\Psi_1(t, x, y, z) = 0$ and $\Psi_2(t, x, y, z) = -\frac{b}{2}z$. We employ a terminal condition $g(x) = -|x_1 - x_2|$. The discretization of the problem is set with $N = 40$. In our first experiment, we set $a = 0.0315$, $b = 0.6$, $x_0 = (-0.1, 0.1)^\top$, and $c = 0$ and use (25) to compute a reference solution. In our second experiment, we set $a = 0.0315$, $x_0 = (-0.1, 0.1)^\top$, $c = 1$ and let b vary between 0.00125 and 5.

For the first experiment, the reference solution is computed with a Monte-Carlo approximation of (25). For the second experiment, we use a finite difference scheme to approximate (24). More specifically, we approximate the solutions on a spatial domain $[-2, 2] \times [-2, -2]$ with artificial Dirichlet boundary conditions.

Results and discussion:

Figure 10 displays the approximate initial condition during training for both the deep BSDE and deep multi-FBSDE methods. The figure clearly illustrates that the deep BSDE method yields inaccurate approximations, whereas the deep multi-FBSDE method produces highly accurate results. For the second experiment, we explore the accuracy of the deep BSDE method and the deep multi-FBSDE method for different values of b . In Figure 11, we see that for $b > 0.25$, the deep BSDE fails to provide accurate approximations. The deep multi-FBSDE method provides accurate approximations for all b tested.

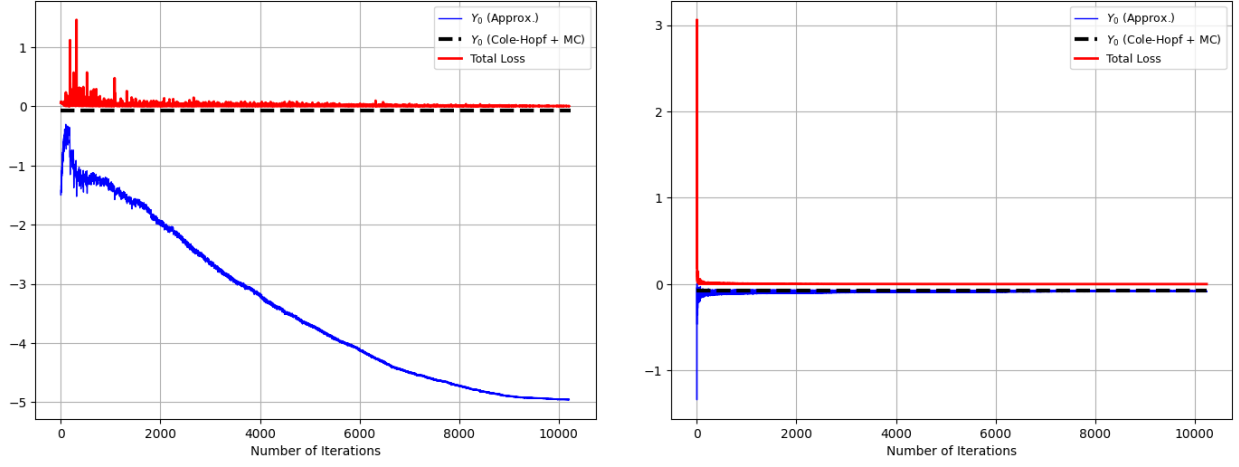


Figure 10: Loss and approximation of Y_0 during training for the deep FBSDE method (left) and the deep multi-FBSDE method (right).

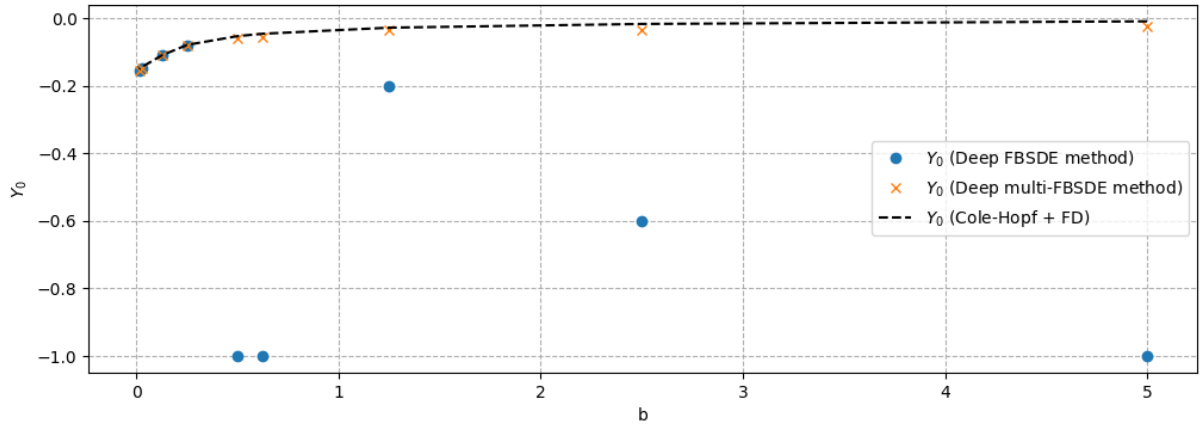


Figure 11: Approximate initial values for different values of b . To no distrort visibility of the plot we have used the maximum of -1 and the approximate initial conditions (Y_0 approximated with the deep BSDE method for $b = 10$, $b = 1.25$ and $b = 1$ is -1.04 , -2.9 and -4.9 respectively).

5 Conclusions and potential future research directions

In this paper, we introduced a two-phase deep-learning-based method, the deep multi-FBSDE method, for approximating coupled forward–backward stochastic differential equations (FBSDEs). Our approach targets scenarios where the standard deep BSDE method of Han, Jentzen, and E (2018) fails to converge. The main characteristic of our method is that its loss function is composed of the sum of multiple deep BSDE loss functions, each originating to a FBSDE satisfying the same partial differential equation (PDE) as the original FBSDE, but with transformed drift and driver. The method was demonstrated on two stochastic control problems and two FBSDEs related to advection diffusion reaction PDEs, unrelated to stochastic control. For neither of the problems, the deep BSDE method worked, but the deep multi-FBSDE method did. Overall, our results suggest that focusing on a family of equivalent FBSDEs offers a promising path to overcome convergence challenges in deep BSDE methods, thus broadening the scope of problems in finance, control theory, and related areas where these methods can be applied effectively.

Although the method seems to work very well on challenging FBSDE, we still do not understand the reason for this and why the deep BSDE method fails. There is thus a need to both understand theoretically for what problems the deep BSDE does not work and why, and why the deep multi-FBSDE method does work for these problems. From a practical perspective, the choice of K and ψ_1, \dots, ψ_K in our algorithm is currently somewhat *ad hoc*. While this works for moderately complex problems, a more systematic approach to selecting K and ψ_1, \dots, ψ_K would be especially beneficial when dealing with high-dimensional systems or models where it is difficult to anticipate the impact of different choices. Developing such a framework constitutes a natural next step toward enhancing both the reliability and the applicability of the proposed method. Furthermore, extending the methodology to broader classes of PDE-driven problems and exploring theoretical guarantees for large-scale or high-dimensional settings would deepen our understanding of its robustness and versatility.

Acknowledgments

Part of this work was carried out during a two-month postdoctoral visit of Kristoffer Andersson (KA) at the University of Utrecht, whose hospitality and support are gratefully acknowledged. KA also acknowledges financial support from RiBa 2022 Research Fund provided by the University of Verona.

References

- [1] Kristoffer Andersson, Adam Andersson, and Cornelis W Oosterlee. Convergence of a robust deep FBSDE method for stochastic control. *SIAM Journal on Scientific Computing*, 45(1):A226–A255, 2023.
- [2] Kristoffer Andersson and Alessandro Gnoatto. Multi-layer Deep xVA: Structural Credit Models, Measure Changes and Convergence Analysis. *arXiv preprint arXiv:2502.14766*, 2025.
- [3] Kristoffer Andersson, Alessandro Gnoatto, Marco Patacca, and Athena Picarelli. A deep solver for BSDEs with jumps. *arXiv preprint arXiv:2211.04349*, 2022.
- [4] Karl J Åström. *Introduction to stochastic control theory*. Courier Corporation, 2012.
- [5] Christian Beck, Sebastian Becker, Patrick Cheridito, Arnulf Jentzen, and Ariel Neufeld. Deep splitting method for parabolic PDEs. *SIAM J. Sci. Computing*, 43(5):A3135–A3154, 2021.
- [6] Christian Beck, Sebastian Becker, Philipp Grohs, Nor Jaafari, and Arnulf Jentzen. Solving the Kolmogorov PDE by means of deep learning. *Journal of Scientific Computing*, 88(3):1–28, 2021.
- [7] Christian Beck, Weinan E, and Arnulf Jentzen. Machine learning approximation algorithms for high-dimensional fully nonlinear partial differential equations and second-order backward stochastic differential equations. *Journal of Nonlinear Science*, 29:1563–1619, 2019.

- [8] Christian Beck, Martin Hutzenthaler, Arnulf Jentzen, and Benno Kuckuck. An overview on deep learning-based approximation methods for partial differential equations. *Preprint arXiv:2012.12348*, 2020.
- [9] Julius Berner, Philipp Grohs, and Arnulf Jentzen. Analysis of the generalization error: Empirical risk minimization over deep artificial neural networks overcomes the curse of dimensionality in the numerical approximation of Black–Scholes partial differential equations. *SIAM Journal Mathematics of Data Science*, 2(3):631–657, 2020.
- [10] Daniel Bussell and Camilo Andrés García-Trillos. Deep multi-step mixed algorithm for high dimensional non-linear PDEs and associated BSDEs. *arXiv preprint arXiv:2308.14487*, 2023.
- [11] Quentin Chan-Wai-Nam, Joseph Mikael, and Xavier Warin. Machine learning for semi linear PDEs. *Journal of Scientific Computing*, 79(3):1667–1712, 2019.
- [12] Dennis Elbrächter, Philipp Grohs, Arnulf Jentzen, and Christoph Schwab. DNN expression rate analysis of high-dimensional PDEs: Application to option pricing. *Constructive Approximation*, pages 1–69, 2021.
- [13] Fang Fang and Cornelis W Oosterlee. A novel pricing method for european options based on fourier-cosine series expansions. *SIAM Journal of Scientific Computing*, 31(2):826–848, 2009.
- [14] Masaaki Fujii, Akihiko Takahashi, and Masayuki Takahashi. Asymptotic expansion as prior knowledge in deep learning method for high dimensional BSDEs. *Asia-Pacific Financial Markets*, 26(3):391–408, 2019.
- [15] Maximilien Germain, Huyen Pham, and Xavier Warin. Approximation error analysis of some deep backward schemes for nonlinear PDEs. *SIAM Journal on Scientific Computing*, 44(1):A28–A56, 2022.
- [16] Philipp Grohs, Fabian Hornung, Arnulf Jentzen, and Philippe von Wurstemberger. *A proof that artificial neural networks overcome the curse of dimensionality in the numerical approximation of Black–Scholes partial differential equations*, volume 284 (1410) of *Memoirs of the American Mathematical Society*. American Mathematical Society, Providence, RI, 2023.
- [17] Jiequn Han, Arnulf Jentzen, and E Weinan. Solving high-dimensional partial differential equations using deep learning. *Proceedings of the National Academy of Sciences*, 115(34):8505–8510, 2018.
- [18] Jiequn Han and Jihao Long. Convergence of the deep BSDE method for coupled FBSDEs. *Probability, Uncertainty and Quantitative Risk*, 5(1):1–33, 2020.
- [19] Pierre Henry-Labordere. Deep primal-dual algorithm for BSDEs: Applications of machine learning to CVA and IM. *Available at SSRN 3071506*, 2017.
- [20] Côme Huré, Huyên Pham, and Xavier Warin. Deep backward schemes for high-dimensional nonlinear PDEs. *Mathematics of Computation*, 89(324):1547–1579, 2020.
- [21] Martin Hutzenthaler, Arnulf Jentzen, Thomas Kruse, and Tuan Anh Nguyen. A proof that rectified deep neural networks overcome the curse of dimensionality in the numerical approximation of semilinear heat equations. *SN partial differential equations and applications*, 1(2):1–34, 2020.
- [22] Arnulf Jentzen, Diyora Salimova, and Timo Welti. A proof that deep artificial neural networks overcome the curse of dimensionality in the numerical approximation of Kolmogorov partial differential equations with constant diffusion and nonlinear drift coefficients. *Communications in Mathematical Sciences*, 19(5):1167–1205, 2021.
- [23] Shaolin Ji, Shige Peng, Ying Peng, and Xichuan Zhang. Three algorithms for solving high-dimensional fully coupled FBSDEs through deep learning. *IEEE Intelligent Systems*, 35(3):71–84, 2020.

- [24] Shaolin Ji, Shige Peng, Ying Peng, and Xichuan Zhang. A control method for solving high-dimensional hamiltonian systems through deep neural networks. *Preprint arXiv:2111.02636*, 2021.
- [25] Yifan Jiang and Jinfeng Li. Convergence of the deep BSDE method for FBSDEs with non-Lipschitz coefficients. *Probability, Uncertainty and Quantitative Risk*, 6(4):391–408, 2021.
- [26] Lorenc Kapllani and Long Teng. A backward differential deep learning-based algorithm for solving high-dimensional nonlinear backward stochastic differential equations. *arXiv preprint arXiv:2404.08456*, 2024.
- [27] Balint Negyesi, Kristoffer Andersson, and Cornelis W Oosterlee. The One Step Malliavin scheme: new discretization of BSDEs implemented with deep learning regressions. *IMA Journal of Numerical Analysis*, 44(6):3595–3647, 2024.
- [28] Maziar Raissi. Forward–backward stochastic neural networks: deep learning of high-dimensional partial differential equations. In *Peter Carr Gedenkschrift: Research Advances in Mathematical Finance*, pages 637–655. World Scientific, 2024.
- [29] Christoph Reisinger, Wolfgang Stockinger, and Yufei Zhang. A posteriori error estimates for fully coupled mckean–vlasov forward-backward sdes. *IMA Journal of Numerical Analysis*, 44(4):2323–2369, 2024.
- [30] Zhipeng Huang, Balint Negyesi, and Cornelis W. Oosterlee. *Convergence of the deep BSDE method for stochastic control problems formulated through the stochastic maximum principle*. Mathematics and Computers in Simulation 227 (2025): 553-568.
- [31] Yutian Wang and Yuan-Hua Ni. Deep BSDE-ML Learning and Its Application to Model-Free Optimal Control. *Preprint arXiv:2201.01318*, 2022.
- [32] Jianfeng Zhang. *Backward stochastic differential equations*. Springer, 2017.